Network Former Mixing Effects in Alkali Germanotellurite Glasses:

A Vibrational Spectroscopic Study

N.S. Tagiara[1], K.I. Chatzipanagis[1], H. Bradtmüller[2,3], A.C.M. Rodrigues[3], D. Möncke[4],

E.I. Kamitsos[1,*]

[1]*Theoretical and Physical Chemistry Institute, National Hellenic Research Foundation,*

48 Vassileos Constantinou Ave., 116 35 Athens, Greece.

[2]*Institut für Physikalische Chemie, Westfälische Wilhelms-Universität, Corrensstr. 30,*
D-48149, Münster, Germany y.

[3]*Department of Materials Engineering, Vitreous Materials Laboratory, Federal University of*
São Carlos, CP 676, 13565-905, São Carlos, SP, Brazil.

[4]*Inamori School of Engineering at the New York State College of Ceramics,*

Alfred University, 1 Saxon Drive, Alfred 14802, New York, USA.

*Corresponding author.

E-mail address: eikam@eie.gr (E.I. Kamitsos)

Abstract: Alkali germanotellurite glasses of composition $0.3M_2O-0.7[(1-x)GeO_2-xTeO_2]$, M=Li, Na and $0{\leq}x{\leq}1$, were investigated by Raman and infrared vibrational spectroscopic techniques to search for the origins of the alkali ion-dependent network former mixing (NFM) effect in these ion-conducting glasses. The vibrational spectra measured on mixed network-former glasses, and the spectral comparison between equimolar-mixed glasses (x=0.5) and pellet-mixtures of the endmember glasses, $0.3M_2O-0.7GeO_2$ and $0.3M_2O-0.7TeO_2$, provided evidence for the formation of hetero-atomic Ge-O-Te linkages and structural rearrangements in the germanate and tellurite components of glass. The mixing-induced structural rearrangements were expressed in terms of chemical equilibria between the network-building units and were used to make qualitative predictions for changes in the network cross-linking density and the related network-strain energy, as well as in the binding energy part of the activation energy for ion conduction. Thus, it is proposed that the mixing-induced structural modifications in the germanate and tellurite parts of glass cause the cancelation of changes in the binding energy and the network-strain energy contributions to the activation energy for ion transport. These qualitative predictions were discussed in the context of the previously found absence of an NFM effect for M=Na and the presence of a weak positive NFM effect for M=Li.

Keywords: *Tellurite glasses, Germanate glasses, Network Former Mixing, Raman spectroscopy, Infrared spectroscopy, Ion-conducting glasses.*

1.   Introduction

Mixing network formers introduces an avenue of changing the topology of glass networks while keeping the network modifier concentrations constant. The concomitant changes of physical properties upon variation of network former ratios, such as ion-conduction and elastic properties are often non-linear and, thus, attract wide interest in the field [1-7]. Over the last decade, several studies have reported network former mixing (NFM) effects in many ternary alkali oxide glass systems [8-11]. Within such systems, an NFM effect is observed when the magnitude of a physical property in the ternary glass deviates from the weighted average of the properties of the binary endmember glasses.

Often, solid-state nuclear magnetic resonance (NMR) spectroscopy is exploited to study NFM effects by offering insights into the short- and intermediate-range structure of such glasses,

i.e., by probing network former connectivity or alkali and alkaline-earth ion distributions. However, there are elements among the oxide glass-formers that do not exhibit favorable NMR properties and, therefore, spectroscopic information is sometimes only available from other spectroscopic or diffraction methods. For instance, in a recent study of GeO_2-TeO_2 mixed network former glasses with composition $0.3M_2O$-$0.7[(1-x)GeO_2$-$xTeO_2]$, where M=Li, Na and $0 \leq x \leq 1$, an alkali-ion-dependent NFM effect was observed for the first time [12]. In particular, the ionic conductivity was found to exhibit a weak positive NFM effect for M=Li but to correspond to the weighted average conductivity values of the binary endmembers in the Na-glass system. The structural origins for these different effects were explored mainly by ^{125}Te solid-state NMR spectroscopy; however, concrete structural evidence could not be derived from the presented NMR data because the resolution of the ^{125}Te NMR experiments was insufficient to obtain meaningful structural information and ^{73}Ge NMR experiments were completely unfeasible. Also, the absence of spectroscopic evidence for the formation of mixed Ge-O-Te linkages led to the tentative proposition that the alkali-ion-dependent NFM effect is related to cation-dependent segregation/phase separation phenomena, which occur for M=Na over a wider distance range than in the Li-containg germanotellurite glasses [12].

Besides NMR spectroscopy, infrared (IR) and Raman vibrational techniques can provide insights into the structural characteristics of glasses and their effect on physical properties. Examples include the probing of both the network structure and the distribution of metal ions, and their correlation with properties like glass transition [13,14] and ion transport [15] in borate glasses, basicity in borate [15] and germanate [16] glasses, and elastic properties in tellurite glasses [17]. In a recent study, a different approach was taken to probe NFM effects in mixed lithium borotellurite glasses, Li_2O-B_2O_3-TeO_2, by comparing weighted average infrared spectra of the endmember binary glasses with the corresponding spectra measured on mixed network former glasses [18]. A similar treatment of the Raman spectra appears promising for application in the otherwise spectroscopically challenging mixed GeO_2-TeO_2 glass system [12].

In the present work, alkali germanotellurite glasses with composition $0.3M_2O$-$0.7[(1-x)GeO_2$-$xTeO_2]$, where M=Li, Na and $0 \leq x \leq 1$, are investigated by employing Raman and IR spectroscopy to shed light on the structures of the germanate and tellurite parts and on their connectivity in forming the glass network. The results are discussed with reference to the recent

NMR study by Bradtmüller et al. on glass samples from the same batch and to the finding that the NFM effect in ionic conductivity is weakly positive for M=Li but absent for M=Na [12].

2. Materials and methods

2.1 Glass preparation and measurements of physical properties

Alkali germanotellurite glasses $0.3M_2O-0.7[(1-x)GeO_2-xTeO_2]$ (M=Li, Na and $0\leq x \leq 1$) were synthesized by conventional melt quenching [12]. Glass compositions in these Li- and Na-germanotellurite series are denoted here by MGTX where M=Li, Na, and X=100x. For each composition, 12 g batches of finely ground Li_2CO_3 (Oregon L.W., 99.99%), Na_2CO_3 (Alfa Aesar, 99.95%), GeO_2 (Alfa Aesar, 99.999%), and TeO_2 (Merck, 99.5%) were mixed, homogenized, and then melted in a platinum crucible using a bottom-loading high-temperature furnace. Melting temperatures in the range 780–1130 °C were employed depending on the composition, and melting times of 30–40 min were chosen. The melts were subsequently splat-quenched on a room temperature stainless-steel plate using a copper block. The resulting glasses were then heat-treated at an annealing temperature of 30 °C below T_g for 12 hours to relieve thermal stresses. After slow cooling to room temperature, the obtained glass specimens were transparent with a yellowish color, which becomes more intense for higher TeO_2 contents. Sodium-containing glasses with high TeO_2 content ($x>0.5$) were hygroscopic and prone to crystallization and thus needed to be re-melted once at the same conditions. After synthesis, all samples were quickly stored in a dry atmosphere.

Glass transition temperatures, T_g, were determined before the annealing process by differential scanning calorimetry (DSC) on bulk pieces in Pt sample pans using a NETZSCH Thermalische Analyse DSC 404 cell, equipped with a TASC 414/3 controller providing a heating rate of 10 °C/min. The measured DSC curves for the studied Li- and Na-containing glasses are shown in Figures 1a and 1b respectively. The T_g values were determined as the onset of the heat capacity steps during the glass transition process as shown in the inset of Figure1a, where the crystallization temperature, T_x, is also marked. The obtained values for T_g and T_x are listed in Table 1 as a function of composition, together with values of glass stability (S) against crystallization. The glass stability is expressed by the difference between the first crystallization onset value and the glass transition temperature, $S=T_x–T_g$. The error in determining T_g and T_x is estimated to be ±1°C, leading to an error in the S value of ±1.5°C.

Glass density was measured by the Archimedes principle, using the density determination kit for solids of a Mettler high-accuracy balance of sensitivity 10^{-5} g [19], and employing toluene as the immersion liquid to avoid glass hydrolysis. For each glass composition, density was measured on at least three different samples resulting in an error of about ±0.004 g/cm^3. The measured density values are reported in Table 1 for the synthesized glasses.
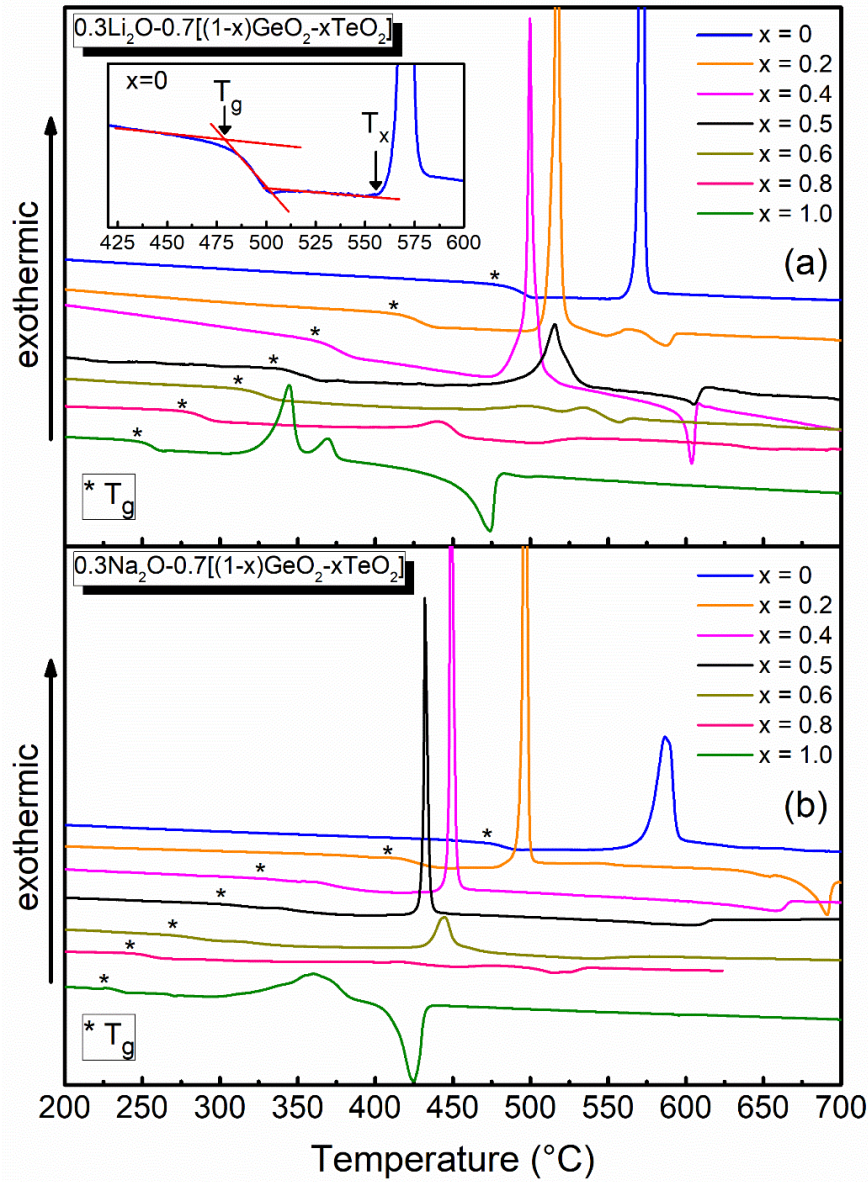

Figure 1. DSC curves for glasses 0.3M$_2$O-0.7[(1-x)GeO$_2$-xTeO$_2$] with M=Li (a), and M=Na (b). The inset in (a) shows in an expanded scale the glass transition event for $x=0$ and the marking of glass transition (T_g) and crystallization (T_x) temperatures.

Table 1. Glass transition temperature (T_g), crystallization temperature (T_x), stability (S), density (ρ), and molar volume (V_m) of glasses $0.3M_2O-0.7[(1-x)GeO_2-xTeO_2]$ (M = Li, Na).

Glass Composition		T_g ± 1 °C	T_x ± 1 °C	S ± 1.5 °C	ρ ±0.004 g/cm^{-3}	V_m ±0.01 cm^3/mol
	$x = 0.0$	476	556	80	3.840	21.40
	$x = 0.2$	410	498	88	4.055	22.16
	$x = 0.4$	361	470	109	4.219	23.13
M=Li	$x = 0.5$	334	473	139	4.303	23.57
	$x = 0.6$	312	483	171	4.391	23.98
	$x = 0.8$	275	420	145	4.549	24.84
	$x = 1.0$	247	310	63	4.669	25.85
	$x = 0.0$	472	556	84	3.689	24.89
	$x = 0.2$	407	474	67	3.890	25.58
	$x = 0.4$	327	438	111	4.054	26.44
M=Na	$x = 0.5$	300	421	121	4.130	26.89
	$x = 0.6$	270	427	157	4.208	27.31
	$x = 0.8$	241	405	164	4.298	28.53
	$x = 1.0$	225	298	73	4.450	29.28

2.2   *Spectroscopic measurements*

Raman spectra were measured at the backscattering geometry on a Renishaw inVia Raman Microscope, equipped with a 2400 lines/mm diffraction grating, a high-sensitivity Peltier-cooled charge-coupled device (CCD), a motorized xyz microscope stage, and a 50x long working distance lens. All spectra were recorded at room temperature with 2 cm^{-1} resolution. The 514.5 nm line of an Ar ion laser was used for excitation employing about 0.10 mW/μm^2 at the glass sample, with no signs of laser-induced modifications being observed. For compositions with x=0, 0.5, and 1 of both glass series, polarized Raman spectra were also recorded under VV and VH polarizations; the first letter indicates the polarization of the exciting laser beam, and the second letter the polarization of the scattered light with V and H indicating vertical and horizontal, respectively.

Infrared (IR) spectra were measured on a vacuum Fourier transform spectrometer (Bruker, Vertex 80v), in quasi-specular reflectance mode (11° off-normal). Reflectance spectra were separately recorded in the far-IR and mid-IR range and then merged to form a continuous spectrum in the range of 30–7000 cm^{-1}. All spectra were measured against a high reflectivity gold mirror at room temperature with 4 cm^{-1} resolution. Analysis of reflectance spectra by Kramers–Kronig transformation yielded the absorption coefficient spectra, $a(v)$, from the expression $a(v) = 4\pi v k(v)$ where v is the infrared frequency in cm^{-1} and $k(v)$ is the imaginary part of the complex refractive index [20].

3. Results

3.1 Glass properties

Table 1 summarizes the bulk properties of the studied glasses. The presently measured densities and glass transition temperatures for the endmember Li- and Na-tellurite glasses are in very good agreement with the reported property values on the same glass compositions [21]. This is also the case for reported density [22,23] and glass transition temperature [24] values for the endmember Li- and Na-germanate glasses.

The composition dependence of thermal properties (T_g, T_x, S) and glass molar volume (V_m=molecular weight/density) is shown in Figure 2. In both systems, T_g decreases in a non-linear way with increasing TeO$_2$ content (Figure 2a,b), similarly as observed in previous studies on mixed B$_2$O$_3$-TeO$_2$ glasses [25]. On the other hand, the behavior of the crystallization temperatures is more complex; for M=Li, T_x values correspond well to the weighted average values of the endmember compositions (endmember interpolation) for $0\leq x\leq0.4$ and deviate to higher values for higher TeO$_2$ contents (Figure 2a). For M=Na, T_x exhibits first a negative deviation from the interpolation of endmember values up to x=0.5, and then a positive deviation for larger x values (Figure 2b). As a consequence of these trends in T_g and T_x, the mixing of GeO$_2$ and TeO$_2$ results in a clear enhancement of glass stability in the entire glass-forming range of the M=Li system (Figure 2c). However, the stability of the Na-glass system first decreases for x<0.3 and then increases at higher TeO$_2$ contents (Figure 2d).

The molar volume is found to vary linearly with composition for M=Li (Figure 2e) and to show a slight negative NFM effect for M=Na (Figure 2f).
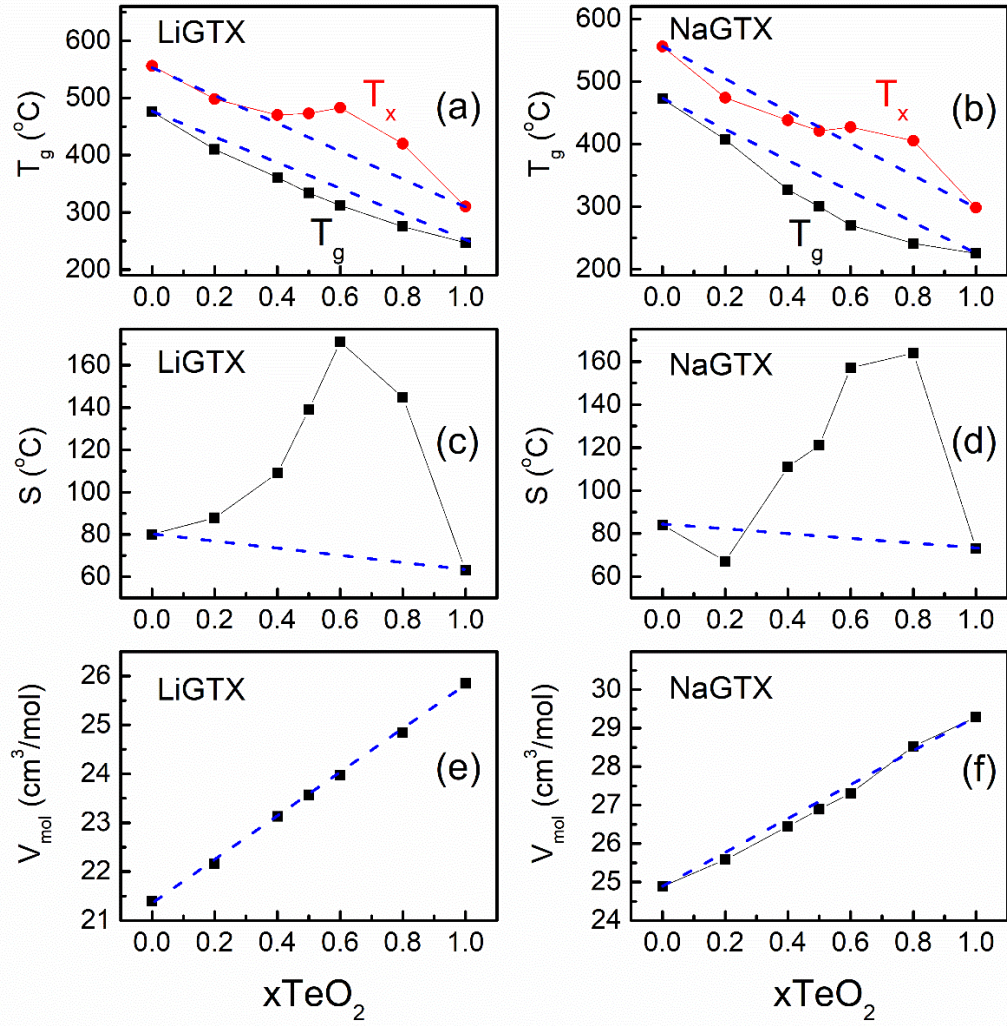
Figure 2. Top (a, b): Glass transition (T_g) and crystallization (T_x) temperatures; Middle (c, d): Glass stability (S), and Bottom (e, f): Molar volume (V_m) for glasses $0.3M_2O-0.7[(1-x)GeO_2-xTeO_2]$ with M=Li (a, c, e) and M=Na (b, d, f). Dashed lines connect the data points of the endmember glasses and serve as guides to the eye in identifying network former mixing effects.

3.2   Glass structure

The Raman and infrared spectra of the sodium- and lithium-germanotellurite glasses are quite similar and can be presented and interpreted jointly. In this context, Figure 3 shows the Raman spectra for both glass systems MGTX (M=Na, Li), and Figure 4 shows the polarized Raman spectra of the binary sodium (lithium) germanate and sodium (lithium) tellurite glasses, as well as those of the mixed network former glasses at maximum mixing (NaGT50 and LiGT50). Figure 5 shows the infrared absorption spectra of MGTX glasses, derived from the specular reflectance

measurements after Kramer-Kronig inversion. In Figure 6 (Raman) and Figure 7 (IR) a comparison is made between the spectra measured on the glasses NaGT50 and LiGT50 and on the equimolar mixtures - in pellet form - of the corresponding endmember glasses ($x=0$ and $x=1$).

3.2.1 Binary alkali-germanate glasses

Starting with the Raman spectra of the binary alkali-germanate glasses $0.3M_2O-0.7GeO_2$ ($x=0$ in Figure 3a,b), we note the presence of dominant band envelopes at 450-650 cm^{-1} and 700-950 cm^{-1}. The first broad and asymmetric envelope, with maximum intensity at 530 cm^{-1} (Na) and 545 cm^{-1} (Li), has been attributed to the symmetric stretching of Ge−O−Ge bridges, v_s(Ge−O−Ge) [26-28]. The shoulder near 605 cm^{-1} (Na) characterizes structures in which GeO_4 tetrahedra and GeO_6 octahedra link to form a three-dimensional network, in analogy to the structure of $Na_4Ge_9O_{20}$ involving Ge_4-O-Ge_6 and Ge_6-O-Ge_6 bridges, where the subscript denotes the coordination number of Ge [26, 27]. Besides the 605 cm^{-1} shoulder, the Raman spectrum of the NaGT0 glass shows weak signals at 325 and 650 cm^{-1} which are also related to GeO_6 octahedra. It is noted that such Raman signatures are not seen in the spectrum of the LiGT0 glass.

The nature of Ge−O−Ge bridges giving rise to the main component of the 530-550 cm^{-1} envelope depends on the alkali content; for low alkali content glasses, these are Ge_4^4-O-Ge_4^4 bridges in four- or three-membered rings made of Ge_4^4 tetrahedra, where the superscript denotes the number of bridging oxygen atoms on Ge. For alkali-rich glasses, bridges of the type Ge_4^4-O-Ge_4^3 are also formed between Ge_4^4 tetrahedra with four bridging oxygen atoms and Ge_4^3 tetrahedra with three bridging and one non-bridging oxygen (NBO) atom; these are known also as Q^4 and Q^3 germanate tetrahedral sites.

The second strongest band envelope is found between 700 and 950 cm^{-1} with a dominant peak at 865 cm^{-1} for M=Na and 850 cm^{-1} for M=Li. This strong peak has been assigned to the symmetric stretching of Ge_4^3 (Q^3) units and involves mainly the stretching of Ge-NBO bonds, Ge-O^- [26-31]. The analogous stretching mode of Ge_4^2 (Q^2) units is active at a lower frequency, around 755-790 cm^{-1} depending on the charge balancing cation, with Q^2 units forming above 20 mol% Li_2O and above ca. 30 mol% M_2O for M=Na, K, Rb, Cs [23, 26-31]. For the NaGT0 glass of this study (Figure 3a, $x=0$), the Q^2 band could correspond to the ca. 775 cm^{-1} feature [23,30,31], which appears as a shoulder of the Q^3 band at 865 cm^{-1}. The second weak shoulder at around 740 cm^{-1} for M=Na was assigned to Ge-O stretching in higher coordinated germanate polyhedra with Ge

atoms in five- and/or six-fold coordination and its intensity was primarily found to change in the order Na>K>Rb≈Cs [31].

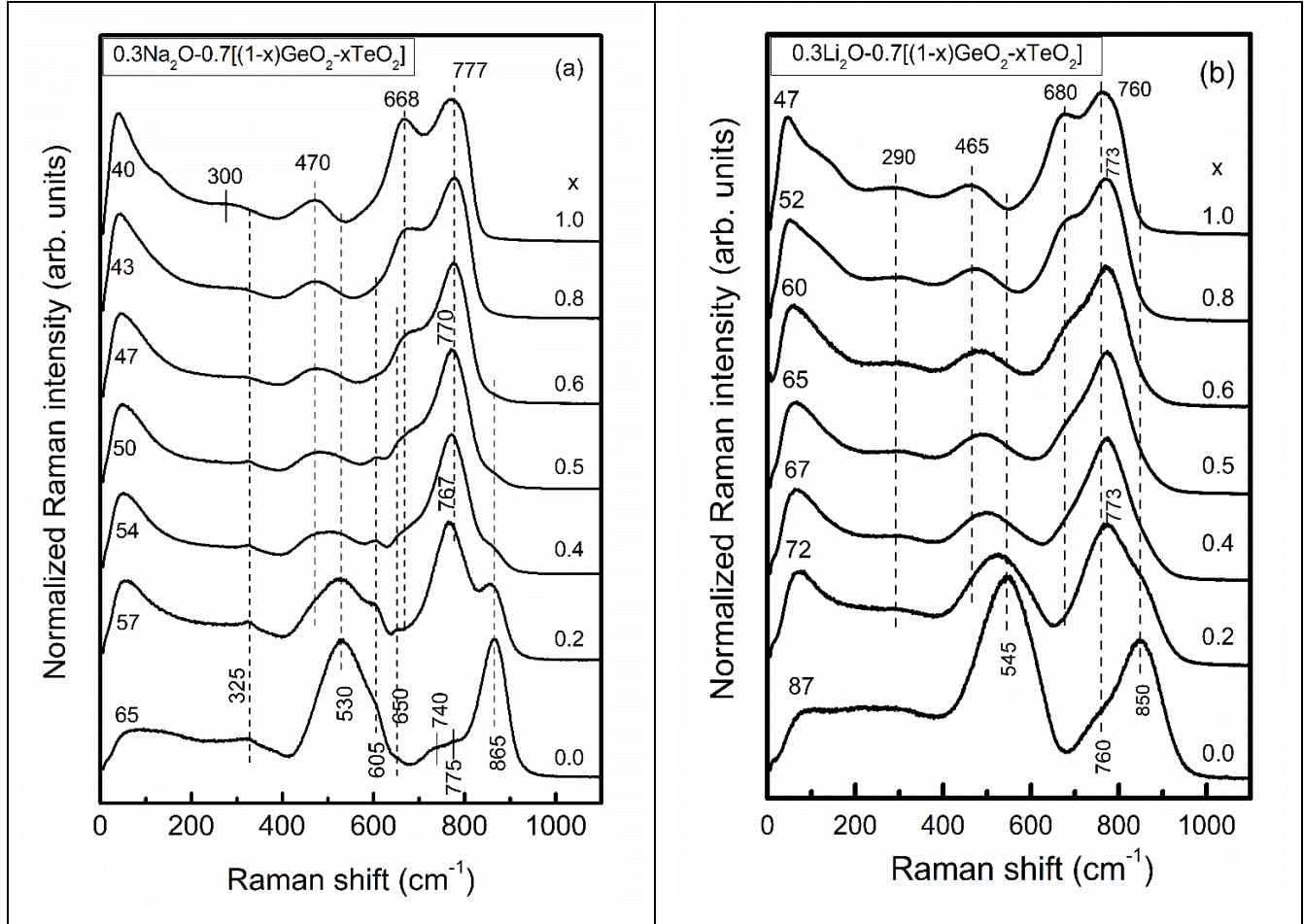**Figure 3.** Raman spectra of sodium (a) and lithium (b) mixed network germanotellurite glass series $0.3M_2O-0.7[(1-x)GeO_2-xTeO_2]$, M=Na, Li and $0\le x \le 1$. The spectra were normalized to their most intense higher frequency band and offset for comparison.

Having associated GeO_6 octahedra with the Raman features at 325, 605, and 650 cm^{-1}, an alternative assignment for the ca. 740 cm^{-1} shoulder for M=Na could be the asymmetric stretching of Q^3 germanate tetrahedral units. To explore this possibility and assist further in assigning Raman and IR bands, we have measured the polarized Raman spectra presented in Figure 4 for the binary ($x=\{0, 1\}$) and ternary ($x=0.5$) germanotellurite glasses $0.3M_2O-0.7[(1-x)GeO_2-xTeO_2]$. As observed in Figure 4a, the spectrum of the NaGT0 glass exhibits strongly polarized Raman features at 325, 530, 605, 650, and 865 cm^{-1}; this suggests their assignment to symmetric vibrational modes.

10

However, the contributions at ca. 740 and 775 cm^{-1} appear depolarized as they retain considerable relative intensity in the VH spectrum, especially concerning the 865 cm^{-1} Q^3 band. Therefore, the 740 and 775 cm^{-1} features may rather be attributable to asymmetric vibrational modes and, as such, are expected to be particularly active in the infrared spectrum. Indeed, the IR spectrum of the NaGT0 glass in Figure 5a shows its stronger band at about 775 cm^{-1}. For Q^3 germanate tetrahedral species with C$_{3v}$ symmetry one would expect the asymmetric stretching mode (v_3) to split into two components, A$_1$(R,IR)+E(R,IR), both being Raman (R) and infrared (IR) active [32]. On these grounds, the IR band at 775 cm^{-1} of NaGT0 could be the convolution of the A$_1$ and E type components of the v_3 mode of Q^3 species, with Raman activities at about 740 and 775 cm^{-1}.
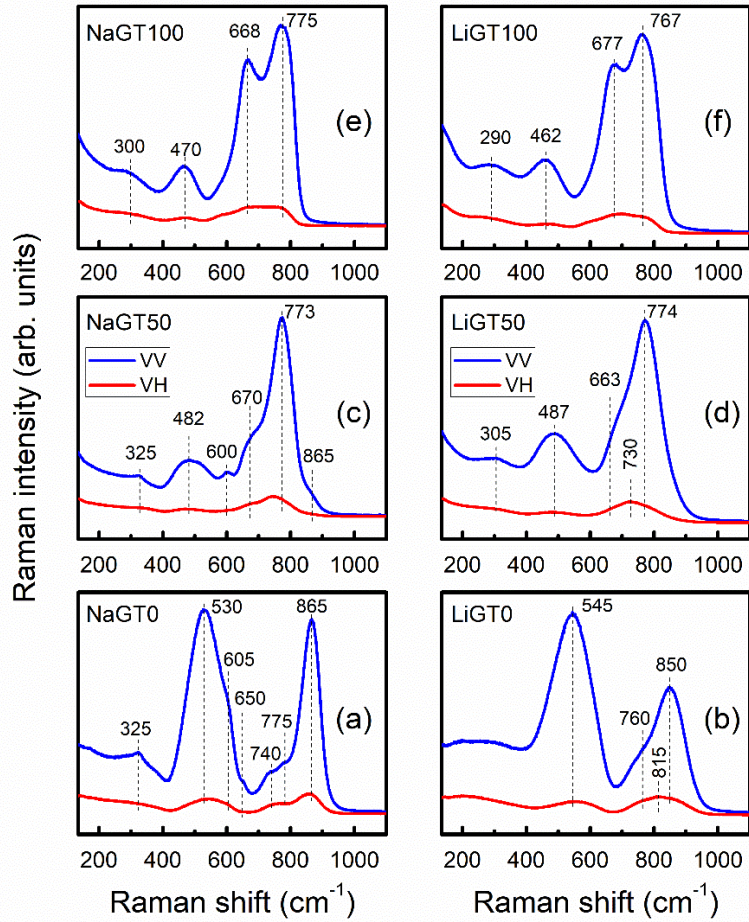

Figure 4. Parallel-polarized (VV, blue) and cross-polarized (VH, red) Raman spectra of binary (a, b, e, f) and ternary (c, d) Na- and Li-germanotellurite glasses 0.3M$_2$O-0.7[(1-x)GeO$_2$-xTeO$_2$], M=Na, Li. The notations NaGTX and LiGTX indicate glass compositions for M=Na and M=Li, respectively, with X being the TeO$_2$ content in mol%, i.e., X=100x.

The VH Raman spectrum of the LiGT0 endmember shows its high-frequency envelope peaking at ca. 815 cm^{-1} (Figure 4b), where the corresponding IR spectrum exhibits its largest intensity ($x=0$ in Figure 5b). This suggests that the v_3 mode of Q^3 germanate species should be active at 815 cm^{-1} for the LiGT0 glass and, thus, its Raman shoulder at about 760 cm^{-1} should be of different origin. Indeed, the Raman feature developing at 760 cm^{-1} for Li_2O contents above 20 mol% was associated with the formation of Q^2 germanate species [23].
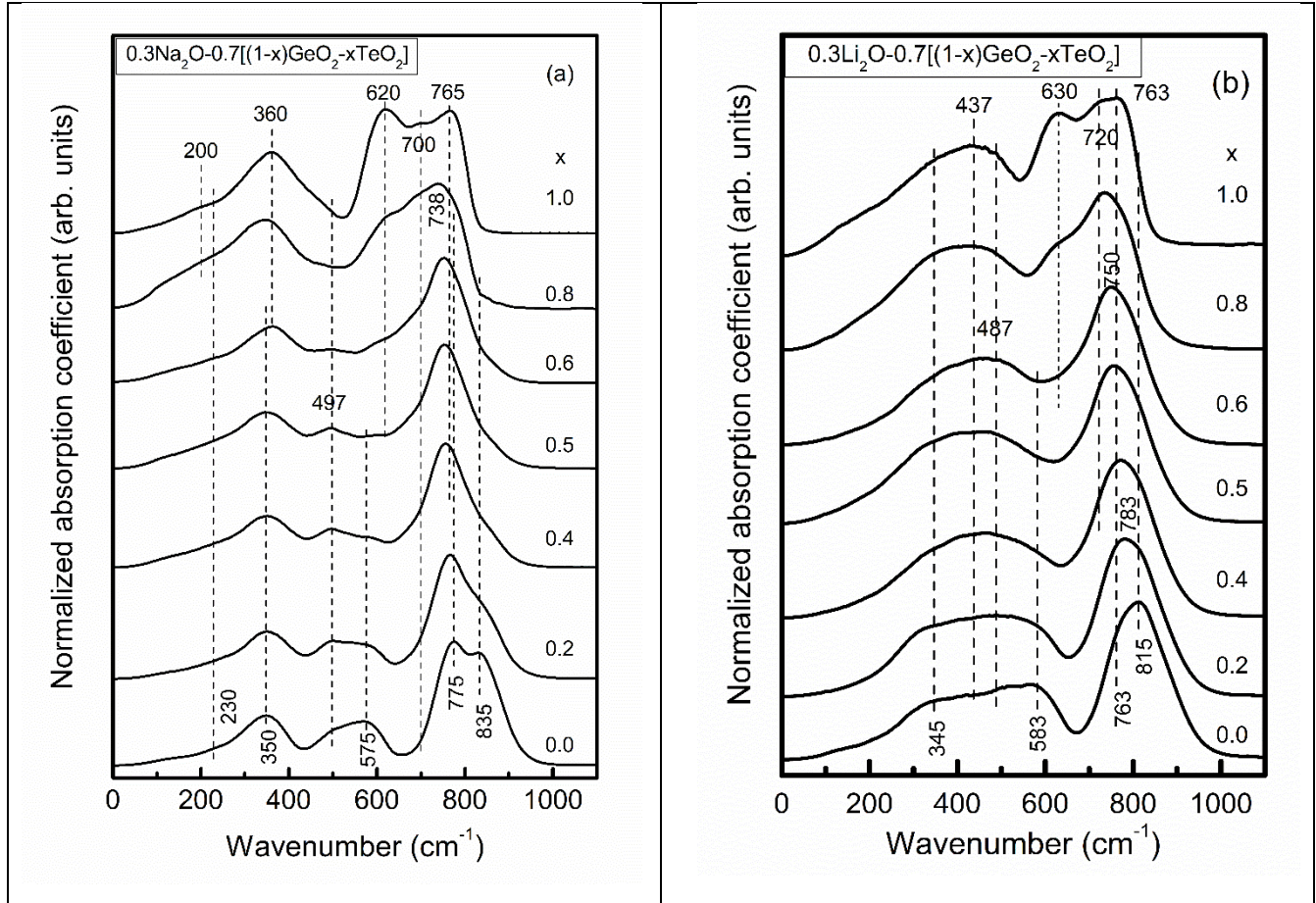

Figure 5. Infrared spectra of sodium (a) and lithium (b) mixed network germanotellurite glasses $0.3M_2O-0.7[(1-x)GeO_2-xTeO_2]$ with M=Na, Li and $0\leq x\leq1$. The spectra were normalized to their most intense higher frequency band and offset for comparison.

The IR spectrum of the NaGT0 glass (Figure 5a, $x=0$) shows better-resolved features at 350 cm^{-1}, around 575 cm^{-1} with a pronounced shoulder at 500 cm^{-1}, and a high-frequency strong envelope with distinct maxima at about 775 and 835 cm^{-1}. Compared to NaGT0, the IR spectrum

of the LiGT0 glass shows considerably broader features (Figure 5b, x=0). According to previous infrared studies on Rb- and K-germanate glasses, and the polarization characteristics of the Raman spectra in Figure 4, the IR bands can be assigned to the rocking motion of Ge-O-Ge bridges near 350 cm^{-1}, to the bending modes of Ge-O-Ge bridges around 450-600 cm^{-1}, to the asymmetric stretching of Q^3 species at 775 cm^{-1} for M=Na and at 815 cm^{-1} for M=Li, and to the asymmetric stretching of Ge-O-Ge bridges around 835 cm^{-1} [26,27,33]. We note also that this high-frequency band at 835 cm^{-1} for NaGT0 encompasses the asymmetric stretching of Ge_4-O-Ge_4 and Ge_4-O-Ge_6 bridges.

The vibrations of Na$^+$ and Li$^+$ ions against their oxide sites, v(M-O), are expected around 200 and 400 cm^{-1} in germanate glasses [34]. The Li-O vibration (~400 cm^{-1}) couples with the Ge-O-Ge rocking mode (~350 cm^{-1}) and the Ge-O-Ge bending mode (500 cm^{-1}) and this gives rise to the broad envelope extending from about 250 to 650 cm^{-1} (Figure 5b). Coupling of vibrational modes has been observed before in glasses with high field strength ions [35]. The Na-O vibration is at lower frequency, around 230 cm^{-1}, and appears as a weak shoulder of the Ge-O-Ge rocking band (Figure 5a).

According to the Dachille and Roy approach [36], the average coordination number (CN) of germanium can be estimated from the position of the high-frequency IR band which results from the convolution of the v_{as}(Ge_4-O-Ge_4) and v_{as}(Ge_4-O-Ge_6) vibrational modes. This approach was applied to Rb- and K-germanate glasses and resulted in the simplified expression K= $5.6\frac{CN}{\lambda^2}$ where λ is the wavelength (in μm) corresponding to v_{as}(Ge−O−Ge) and K takes the value K=0.172 [26,27,33]. Using for v_{as}(Ge-O-Ge) the band maximum observed at 835 cm^{-1} for the NaGT0 glass (Figure 5a), we estimate an average Ge coordination number of CN(Ge)=4.4. Although our Raman spectrum of this glass indicates that the higher coordination state of Ge is six-fold, the presence of five-fold coordinated germanate species cannot be excluded. The IR spectrum of the LiGT0 glass has no resolved component at the high-frequency side of the 815 cm^{-1} band (Figure 5b), suggesting the absence of Ge_4-O-Ge_6 bridges or a very small content of GeO_6 units in this glass. This is in agreement with the absence of Raman features at about 325, 605, and 650 cm^{-1} which would designate the presence of GeO_6 species (Figure 3b).

As presented above, the presence of Ge in six-fold coordination in glass NaGT0 was inferred from the IR spectrum by considering the influence of Ge_6 on the v_{as}(Ge−O−Ge) mode. The stretching modes of Ge-O bonds in GeO_6 octahedra in the infrared are expected at frequencies

similar to the bending mode of Ge-O-Ge bridges, i.e. around 500 to 650 cm^{-1} [37,38]. In the infrared study of crystalline LiCrGeO$_4$, a band at 447 cm^{-1} was assigned to Li-O stretching for tetrahedral coordinated Li$^+$ ions, and bands at 526 and 623 cm^{-1} were associated with GeO$_6$ octahedral units. The absence of IR bands at higher frequencies was taken to indicate the absence of tetrahedral GeO$_4$ species in this germanate crystal.

In summary, the Raman and IR spectra of the 0.3Na$_2$O-0.7GeO$_2$ glass (NaGT0) show that the germanate network involves tetrahedral Q^3 units and octahedral GeO$_6$ units, while the results for the 0.3Li$_2$O-0.7GeO$_2$ glass (LiGT0) are consistent with the presence of tetrahedral Q^3 and Q^2 units. The preferences of Na$^+$ ions for GeO$_6$ units and of Li$^+$ ions for Q^2 units reflect their difference in ionic field strength.

3.2.2 Binary alkali-tellurite glasses

The Raman spectra of the pure sodium- and lithium-tellurite glasses 0.3M$_2$O-0.7TeO$_2$ (x=1 in Figures 3a and 3b) agree well with published spectra on the same or similar tellurite glass compositions [17-19, 39]. They exhibit a high-frequency envelope with peaks at 668/680 cm^{-1} and 777/760 cm^{-1} for M=Na/Li, and bands with lower intensity at 470/465 cm^{-1} and ca. 300 cm^{-1}. Band assignments follow earlier publications and reflect a partially modified tellurite network [17-19, 39-43]. In particular, the highly polarized peak at 668/677 cm^{-1} (Figures 4e and 4f) is due to the remaining TeO$_4$ trigonal pyramids (tbp's), as it results from the symmetric stretching/breathing mode of Te-O$_2$-Te double bridges, v_s(Te-O$_2$-Te), connecting TeO$_4$ units [43]. The higher intensity peaks at 775/767 cm^{-1} are also polarized and are due to the symmetric stretching of TeO$_{3+1}$ polyhedra with contribution from TeO$_3$$^{2-}$ trigonal pyramids (tp's) with three terminal oxygen atoms. The notation TeO$_{3+1}$ indicates a tbp unit with one terminal oxygen atom and three bridging oxygen atoms, with one bridging Te-O bond being comparatively longer than the other three Te-O bonds [44]. The weaker component at 470/462 cm^{-1} arises from the stretching-bending vibration of Te-O-Te single bridges, and the very weak contribution at about 300 cm^{-1} from O-Te-O bending [43]. As observed in Figures 4e and 4f, the above Raman peaks are also polarized suggesting their association with symmetric vibrational modes.

While the Raman spectra of Na- and Li-tellurite glasses are dominated by symmetric stretching and bending vibrations of tellurite species, the corresponding asymmetric vibrational modes are strongly active in the infrared (x=1 in Figures 5a and 5b). Thus, the presence of TeO$_4$

units is signaled by the 620/630 cm^{-1} peak, TeO$_{3+1}$ units by the ca. 700/720 cm^{-1} feature, and TeO$_3^{2-}$ units by the higher-frequency contribution at 765/763 cm^{-1}. The asymmetric stretching-bending mode of Te-O-Te bridges is observed around 360 cm^{-1} for M=Na. The analogous mode for the Li-tellurite glass overlaps with the Li-oxygen vibration at a higher frequency, resulting in the broad envelope peaking at about 430 cm^{-1}.

3.2.3   Ternary alkali-germanotellurite glasses

The Raman spectra of mixed former glasses 0.3M$_2$O-0.7[(1-x)GeO$_2$-xTeO$_2$] show that the most pronounced changes occur when the second former oxide is added to the binary glass, that is for $0 \leq x \leq 0.2$ and $0.6 \leq x \leq 1.0$ (Figure 3). Starting with TeO$_2$ addition, a quite drastic decrease in intensity is noted for the Q^3 germanate band at 865/850 cm^{-1} with the parallel appearance of a disproportionally strong tellurite band at 767/773 cm^{-1} (x=0.2 in Figures 3a and 3b). Such large differences in Raman intensity between the tellurite and germanate species should result from the considerably higher polarizability, α, of the Te^{4+} ion compared to Ge^{4+}, with $\alpha_{Te^{4+}}$=1.595 Å^3 and $\alpha_{Ge^{4+}}$=0.137 Å^3 [45]. Since the Raman intensity is proportional to the square of the polarizability derivative with respect to the normal coordinate of the mode, the Raman cross-section of tellurite vibrations would be significantly larger compared to germanate-related modes. Consequently, even a small number of tellurite species in a germanate matrix is expected to give relatively strong Raman signals. Likewise, small to medium GeO$_2$ contents in mixed germanotellurite glasses would be easily overlooked in the Raman spectra. Indeed, the signature of the Q^3 germanate band at 865/850 cm^{-1} is not noticed for glasses $0.6 \leq x < 1.0$, i.e. for germanate contents lower than about 50% GeO$_2$ (Figure 3).

In addition to polarizability-related effects, the Raman spectra of the Te-rich glasses show that incorporation of GeO$_2$ induces significant changes in the tellurite speciation for both glass series. This is manifested by the reduction in intensity of the TeO$_4$ band at 668/680 cm^{-1} relative to the envelope at about 770 cm^{-1}. The latter becomes progressively more symmetric with increasing GeO$_2$ content, and for M=Na it shifts from 777 to 767 cm^{-1} (Figure 3a). Of interest is also the composition dependence of the tellurite band at 470/465 cm^{-1} (bending of Te–O–Te linkages) which is observed already at x=0.2 as shoulder of the germanate band at 530/545 cm^{-1}, thus signaling the build-up of the tellurite sub-network.

Similar trends are seen in the IR spectra, where the 620/630 cm^{-1} TeO$_4$ band loses intensity and the high-frequency envelope (700-765 and 720-763 cm^{-1}) gains relative intensity upon GeO$_2$ addition (Figures 5a and 5b). Also, the high-frequency envelopes appear to shift to lower frequencies by losing progressively intensity from their high-frequency side. These changes in Raman and IR spectra point to a progressive restructuring of the tellurite sub-network upon addition of GeO$_2$. The combined spectroscopic results indicate the conversion of TeO$_4$ to TeO$_{3+1}$ and the parallel reduction in the population of TeO$_3^{2-}$ units in the presence of GeO$_2$.

Focusing again on the germanate part of the network, we note for both glass-series that even small additions of TeO$_2$ (x=0.2) result in pronounced intensity reduction for the bands at 865/850 cm^{-1} (Q^3) and 530/545 cm^{-1} (Ge−O−Ge). While this manifests the more than 10 times higher polarizability of Te^{4+} over Ge^{4+} ions, the Raman spectra of the Na-series (Figure 3a) demonstrate also a contrasting relative enhancement of the GeO$_6$-related bands at ca. 325 and 605 and 650 cm^{-1} upon increasing TeO$_2$ content. Remarkably, the 325 and 605 cm^{-1} bands are clearly observable even at x=0.6, whereas the 650 cm^{-1} germanate feature merges with the remaining TeO$_4$ intensity at about 670 cm^{-1}. On the contrary, the 865 cm^{-1} (Q^3) band has almost vanished at x=0.6. These findings suggest that GeO$_6$ octahedra are favored over Q^3 tetrahedral units when TeO$_2$ is present in the Na-glass series.

As noted above, GeO$_6$-related bands were not observed in the Raman spectra of the Li-series. Instead, Li$^+$ ions favor their isomeric Q^2 tetrahedral units which give Raman scattering at about 760 cm^{-1}. However, the intensity development at about 760 cm^{-1} upon TeO$_2$ addition (Figure 3b) cannot be attributed entirely to the creation of Q^2 germanate units because tellurite species also scatter at the same frequency range.

The IR spectra of the mixed germanotellurite glasses show mostly the expected evolution as TeO$_2$ replaces GeO$_2$. In addition, we note the gradual emergence of the 497 cm^{-1} feature in the Na-series which is seen at maximum mixing (x=0.5, Figure 5a). Considering that the bending vibration of Te-O-Te bridges is active at 360 cm^{-1} and that for Ge-O-Ge bridges at 575 cm^{-1}, it is reasonable to associate the 497 cm^{-1} feature with the formation of mixed Ge-O-Te bridges upon network former mixing. The situation is less clear in the Li-series because the IR spectra of the corresponding binary glasses show much broader bands in the bridge-bending regions compared to Na-glasses (Figure 5b). Nevertheless, the evolution of absorption at about 487 cm^{-1} upon mixing is compatible with the formation of Ge-O-Te bridges in the Li-series as well.

In summary, the Raman and infrared spectra of the mixed alkali-germanotellurite glasses demonstrate the development of interactions between the GeO_2 and TeO_2 components which lead to structural rearrangements in the germanate and tellurite subnetworks. In addition, infrared spectroscopy gives evidence for mixed Ge–O–Te bonding in both glass series.

3.2.4 *Equimolar-mixed alkali-germanotellurite glasses*

In the context of the present findings, it is clear that mixing the two network former oxides triggers structural rearrangements within the tellurite and germanate sub-networks in both glass series. To explore this aspect further we focus here on the glasses with equimolar mixing and compare spectra measured on the glasses NaGT50 and LiGT50 against pellet-samples made from equimolar amounts of the endmember glasses ($x=0$ and $x=1$). For the latter samples we prepared equimolar mixtures of the corresponding binary glasses, i.e. $(0.3Na_2O-0.7TeO_2)+(0.3Na_2O-0.7GeO_2)$ and $(0.3Li_2O-0.7TeO_2)+(0.3Li_2O-0.7GeO_2)$. For each sample, weighted equimolar amounts of the binary glasses were ground to fine powder and mixed very thoroughly. Each mixture was then pressed into a free-standing pellet with fairly smooth surface. Raman and IR spectra were measured on the pellets and are compared in Figures 6 and 7 with the corresponding spectra of glasses NaGT50 and LiGT50.

The most profound effect of network mixing on the Raman spectra is the intensity reduction of the 667/680 cm^{-1} band from pellets to glasses (Figure 6), indicating an analogous reduction in the relative population of TeO_4 units. Due to polarizability differences, germanate-relate peaks are weak in the Raman spectra of both pellets and glasses. Nevertheless, the Raman spectrum of the NaGT50 glass in Figure 6a shows the 325 and 607 cm^{-1} peaks enhanced relative to the 865 cm^{-1} shoulder in comparison to glass NaGT0, thus suggesting an increased population of GeO_6 octahedral units relative to Q^3 tetrahedral units. A comparison shows that the TeO_4 band at 680 cm^{-1} for glass LiGT50 (Figure 6b) is not reduced to the same extent as for glass NaGT50. This suggests a smaller reduction in the population of TeO_4 units and/or an enhanced scattering at about 760 cm^{-1} due to creation of additional Q^2 germanate units in glass LiGT50.
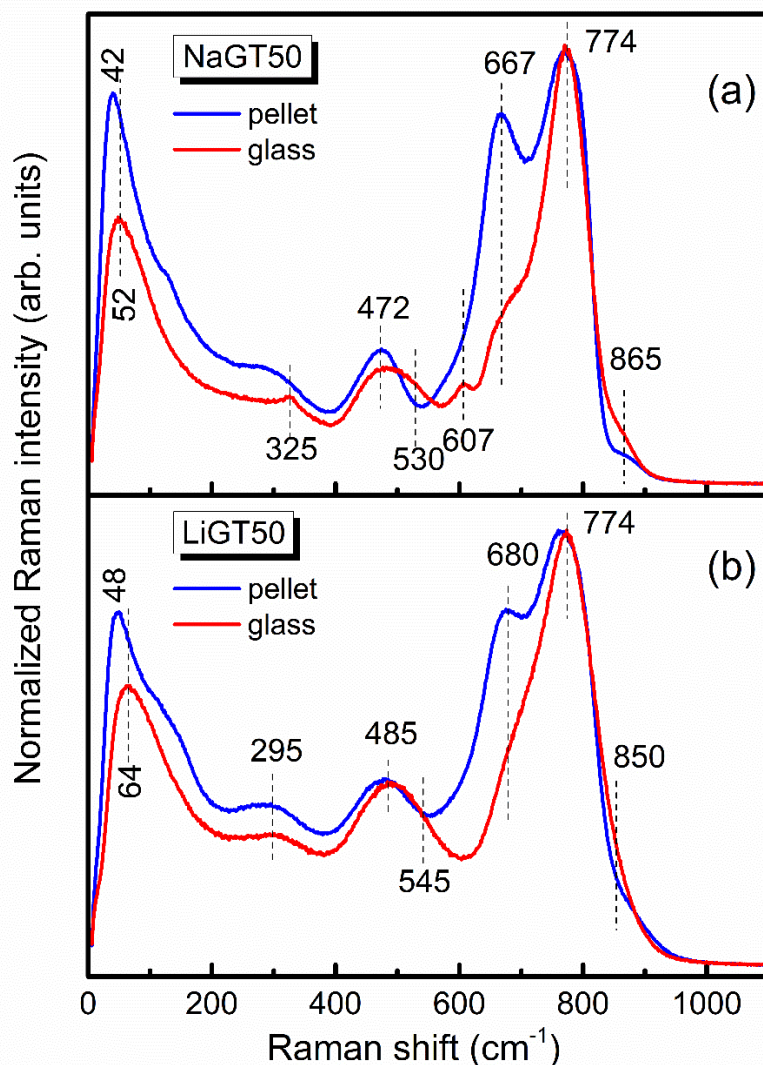
Figure 6. Comparison of the Raman spectra measured on the synthesized glasses and pellets of equimolar mixtures of the corresponding endmember glasses for NaGT50 (a), and LiGT50 (b). The spectra were normalized to their most intense higher frequency band. For details see text.

The infrared spectra of pellet samples in Figure 7 show a band at 600/610 cm^{-1} which is not observed as a distinct band in the spectra of the individual endmember glasses (x=0 and 1 in Figure 5). This band may result from the convolution of the TeO$_4$ band at 620/630 cm^{-1} and the Ge-O-Ge band at 575/583 cm^{-1}, and its near absence in the spectra of glasses NaGT50 and LiGT50 signals the population reduction of TeO$_4$ units and/or Ge-O-Ge bridges upon mixing the two network formers. The destruction of Ge-O-Ge bridges is in line with the intensity reduction at 835/875 cm^{-1} from pellets to glasses (Figure 7). Similar destruction of Te-O-Te bridges in glass

NaGT50 is suggested by the intensity reduction at 355 cm^{-1} (Figure 7a). On the other hand, the spectrum of this glass shows intensity enhancement at 495 cm^{-1} which would be consistent with the formation of mixed Ge-O-Te bridges upon mixing. Analogous observations cannot be made for glass LiGT50 because of the broad nature of the 200-600 cm^{-1} envelope. Finally, the high-frequency IR peak at 774/790 cm^{-1} for pellets shows a clear downshift to 755 cm^{-1} in glasses. This shift signals the decrease in the population of different germanate structure units like Ge-O-Ge bridges and Q^3 germanate tetrahedra. It is consistent also with the destruction of TeO$_3^{2-}$ in favor TeO$_{3+1}$ units, considering that TeO$_{3+1}$ units absorb at lower frequency compared to TeO$_3^{2-}$.
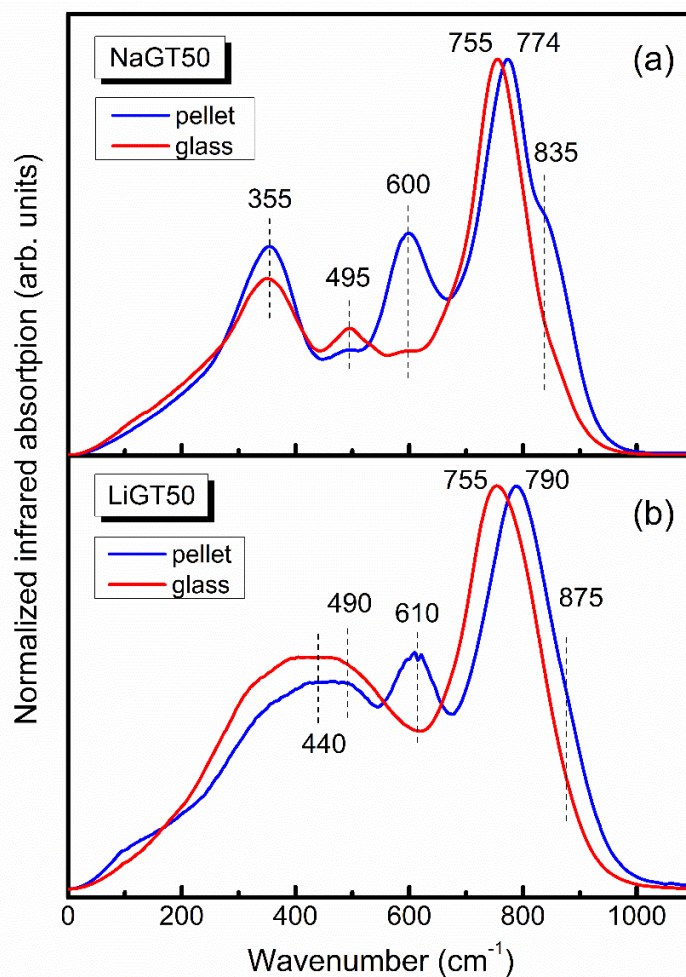

Figure 7. Comparison of the IR spectra measured on glasses and pellets of equimolar mixtures of the corresponding endmember glasses for NaGT50 (a), and LiGT50 (b). The spectra were normalized to their most intense higher frequency band. For details see text.
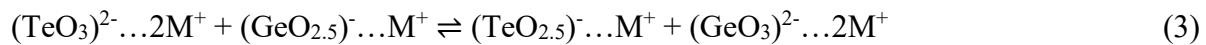
In summary, the Raman and IR spectra of equimolar-mixed alkali-germanotellurite glasses have shown that the structure of mixed glass networks cannot be described as weighted averages of the structures of the binary endmember glasses.

4. Discussion

4.1 Germanate-tellurite interactions in Li(Na)-germanotellurite glasses

The recent NMR study of mixed Li(Na)-germanotellurite glasses indicated a proportional sharing of the alkali cations between the two network former components [12]; this implies a constant degree of modification for each network former across the ternary glass series ($0<x<1$). The consideration of the Raman and infrared spectra of these glasses (Figures 3, 5) and of the equimolar-mixed NaGT50 and LiGT50 glasses and pellets (Figures 6, 7) have demonstrated the development of interactions between the germanate and tellurite components. As a result, the structure of a mixed Li(Na)-germanotellurite glass cannot be described as a weighted average of the structures of the binary endmember glasses. The interactions between the two glass components lead to the formation of mixed Ge-O-Te linkages and the parallel destruction of homo-atomic Ge-O-Ge and Te-O-Te bridges. This tendency promotes the formation of homogeneous glasses upon mixing rather than segregation or phase separation phenomena, at least with length scales detectable by Raman and IR spectroscopy.

Mixing was found to cause also redistribution in the population of germanate and tellurite units in both glass series. Specifically, the addition of TeO_2 was found to favor the transformation of tetrahedral Q^3 units to octahedral GeO_6 units in mixed NaGTX glasses, and to tetrahedral Q^2 units in mixed LiGTX glasses. On the other hand, addition of GeO_2 leads to the conversion of TeO_4 units to TeO_{3+1} polyhedra and to population reduction of $TeO_3{}^{2-}$ units. Considering that the stoichiometry of the TeO_4 unit is $TeO_{4/2}$ and $TeO_{3+1}=(TeO_{2.5})^-$, and the stoichiometry of germanate units is $(GeO_{2.5})^-$ for Q^3, $(GeO_{6/2})^{2-}$ for GeO_6 and $(GeO_{2/2}O_2)^{2-}$ for Q^2, the observed structural changes upon mixing can be expressed by the chemical equilibria:

$$O_{3/2}Ge\text{-}O\text{-}GeO_{3/2} + O_{3/2}Te\text{-}O\text{-}TeO_{3/2} \rightleftharpoons 2[O_{3/2}Ge\text{-}O\text{-}TeO_{3/2}] \tag{1}$$

$$TeO_{4/2} + (TeO_3)^{2-}...2M^+ \rightleftharpoons 2[(TeO_{2.5})^-...M^+] \tag{2}$$

$$(TeO_3)^{2-}...2M^+ + (GeO_{2.5})^-...M^+ \rightleftharpoons (TeO_{2.5})^-...M^+ + (GeO_3)^{2-}...2M^+ \tag{3}$$

Equation (1) describes the formation of mixed Ge-O-Te bridges, Eq. (2) expresses the mixing-induced rearrangement among tellurites units, and Eq. (3) manifests the change in the degree of modification of the two components; the changes in modification expressed by Eq. (3) is in line with the basicity difference between the two glass-forming oxides; i.e., TeO_2 is considerably more basic than GeO_2. In fact, TeO_2 is the most basic among the known glass-forming oxides having $\Lambda(TeO_2)$=0.99 [45], where Λ is the optical basicity. On the other hand, GeO_2 is less basic and its basicity depends on the coordination number of Ge, with $\Lambda(GeO_2)$=0.61 for CN(Ge)=4 and $\Lambda(GeO_2)$=0.40 for CN(Ge)=6 [16].

The $(GeO_3)^{2-}$ species in Eq. (3) represents the GeO_6 or the Q^2 unit, noting that the latter units are chemical isomers:

$$(GeO_{6/2})^{2-} \rightleftharpoons (GeO_{2/2}O_2)^{2-} \tag{4}$$

The above equilibrium is shifted to the left for M=Na and to the righr for M=Li.

4.2   *Structure-ionic conductivity correlation in Li(Na)-germanotellurite glasses*

As noted in the introduction, the composition dependence of ionic conductivity in glasses MGTX (M=Li, Na) shows a weak positive network former mixing (NFM) effect for M=Li and a nearly linear variation for M=Na, i.e. absence of NFM effect, with the conductivity of NaGTX glasses following the weighted average values of the binary endmembers [12]. The difference in the coordination number of germanium in the isomers of Eq. (4) has a direct consequence on the distribution of the two formal negative charges; they are delocalized on the entire octahedral $(GeO_{6/2})^{2-}$ unit i.e. over the six germanium-oxygen bonds but are localized on the two non-bridging oxygen atoms of the $(GeO_{2/2}O_2)^{2-}$ tetrahedral unit. A redistribution of the negative charge over larger network segments will reduce the Coulomb forces between M^+ ions and their anionic sites and, thus, this will facilitate ion transport in mixed M-germanotellurite glasses. An analogous mechanism was discussed for Na- and Li-borophosphate glasses, where replacement of non-bridging P–O$^-$ bonds by the tetrahedral $(BO_4)^-$ groups was found to favor Na/Li ion conduction [2, 3]. On these grounds, the presence of $(GeO_{6/2})^{2-}$ species for M=Na is suggested to be beneficial for ionic conduction in contrast to $(GeO_{2/2}O_2)^{2-}$ species for M=Li. For the same reasoning, and given

Eqs. (2) and (3), the transformation of the doubly charged $(TeO_3)^{2-}$ tellurite species to singly charged $(TeO_{2.5})^-$ species is expected to have a positive effect on ionic conduction in both glass series.

According to the Anderson and Stuart model for ion conduction in glasses [46], there are two main contributions to the activation energy for conductivity, E_σ; the Coulomb binding energy of the ion in its site, E_B, and the elastic strain energy, E_S, associated with the distortion of the glass network as the ion jumps from one equilibrium site to the next one. Based on the previous discussion, the structural changes induced by mixing of GeO_2 with TeO_2 are expected to reduce E_B for the tellurite part in both glass systems and the germanate part of the Na-containing glasses, but to increase E_B for the germanate part of the Li-containing glasses. The network strain energy, E_S, is given from the expression:

$$E_S = 4\pi G r_D (r-r_D)^2 \tag{5}$$

where G is the shear modulus of the glass and r_D is a doorway radius that needs to be enlarged to accommodate an ion of radius r. In the absence of measured values of the shear modulus that would allow the calculation of E_S, we discuss here changes in the network strain energy in terms of changes in the cross-linking density of the glass network by comparing the structural units found in the two glasses series and their efficiency in cross-linking the network. This is because the shear modulus G increases with increasing cross-linking density of the glass network [47, 48].

The structural changes involved in Eq. (1) show no variation in network cross-linking upon mixing. Considering that the number of bridging Te-O bonds (Te-O_b) in units $TeO_{4/2}$, $TeO_{3+1}=(TeO_{2.5})^-$ and $(TeO_3)^{2-}$ is four, three, and zero respectively, the combination of Eqs. (2) and (3) indicates that the number of Te-O_b bonds increases from 4(Te-O_b)/3Te to 9(Te-O_b)/3Te, thus predicting an increased tellurite cross-linking upon mixing for both glass series. In Eq. (3) the germanate speciation changes from to $(GeO_{2.5})^-$ to $(GeO_3)^{2-}$, and thus the change in germanate connectivity will be eventually dictated by Eq. (4). For M=Na, the change from $(GeO_{2.5})^-$ to $(GeO_{6/2})^{2-}$ will increase the number of bridging Ge-O_b bonds by 3(Ge-O_b)/Ge. The opposite effect is foreseen for M=Li, i.e., a decrease by one (Ge-O_b) per Ge. Taken together the changes in the tellurite and germanate connectivity, mixing the two glass former-oxides will leave the network cross-linking density practically unaffected for M=Li but clearly increased for M=Na. Variations

in network cross-linking density are usually reflected in the composition dependence of molar volume, V_{mol}. It was found that V_{mol} varies linearly with composition for M=Li and shows negative deviation from additivity for M=Na (Figures 2e and 2f); this provides support for the predicted change in the network cross-linking density of the two glass series.

A study of ionic conductivity in alkali-germanate glasses has shown that the strain energy component of E_σ is relatively more important for germanate glasses than for the analogous silicates [49, 50]. It was also discussed that the conversion of GeO_4 to GeO_6 units, and the subsequent changes in the medium-range structure, correlate with the increased strain of the network and the reduction in the volume available for the diffusion of the alkali ions; these factors contribute to the increase in E_σ. The importance of the strain energy was also discussed for sodium tellurite glasses, and its contribution to the activation energy for ion conduction was found considerably larger than that of the binding energy [44]. Similarly, the decrease in Ca ion diffusivity with increasing Na content in Na_2O-CaO-B_2O_3 glasses was correlated with the increase in the atomic packing density as BO_3 units are converted into BO_4 units; this leads to the increase in the mechanical strain of the network and affects the ionic transport [51]. In line with this is also the composition dependence of the glass hardness, which was found to follow closely the formation of BO_4 units in the same glass system [51]. Finally, a thorough investigation of sodium-borosilicate and sodium-borogermanate mixed glass systems showed that ionic conductivity and bulk modulus exhibit opposite trends in terms of slopes and extrema in their composition dependence [6], and highlighted the fact that high network cross-linking density and mechanical stiffness is likely related to low ion mobility.

Based on the previous discussion and related literature reports, we summarize for convenience in Table 2 our predictions for the effect of mixing on the electrostatic part, E_B, and the network-strain part, E_S, of the activation energy for ion conduction, $E_\sigma = E_B + E_S$, with reference to both the tellurite and germanate parts in glasses MGTX (M=Li, Na). Taking as an example the Na-containing glasses, Table 2 shows that glass-former mixing will decrease E_B for the tellurite part and increase E_S, thus leaving E_σ (i.e. $E_B + E_S$) practically unchanged for tellurite species. Similarly, the effect of mixing on the germanate part for M=Na will be the decrease in E_B and the increase in E_S and thus E_σ will be practically unchanged for germanate species. While the actual magnitudes of the energy changes are not known in these glasses and the presented description is purely qualitative, the predicted changes in E_B and E_S appear to cancel out for both glass series,

although for different structural reasons. This prediction is in accordance with the experimental finding for the absence of a strong network former mixing effect in both glass systems; the effect is absent in glasses NaGTX and very weak in glasses LiGTX [12].

Table 2. Qualitative description of the mixing-induced changes in the electrostatic, E_B, and network-strain, E_S, part of the activation energy for ion conduction, E_σ, for glasses $0.3M_2O\text{-}0.7[(1\text{-}x)GeO_2\text{-}xTeO_2]$ (M=Li, Na). The predicted energy changes refer to the tellurite and germanate parts of glass and are designated by arrows to indicate the increase (↑) and decrease (↓) in energy. For details, please refer to the text.

Glass	Component	ΔE_B	ΔE_S	ΔE_σ
M=Li	tellurite	↓	↑	≈ 0
	germanate	↑	↓	
M=Na	tellurite	↓	↑	≈ 0
	germanate	↓	↑	

5.   Conclusions

Lithium and sodium germanotellurite glasses with composition $0.3M_2O\text{-}0.7[(1\text{-}x)GeO_2\text{-}xTeO_2]$, where M=Li, Na, and $0 \leq x \leq 1$, were investigated by density and glass transition temperature measurements and by Raman and IR spectroscopy to probe the structure of the germanate and tellurite units, and their (inter)connectivity in building up the mixed glass network. The aim of this work was to search for the underlying origins of the alkali ion-dependent network former mixing (NFM) effect in ionic conductivity of the investigated glasses.

The results of the complementary Raman and IR spectroscopic techniques show mixing-induced interactions between the GeO_2 and TeO_2 oxides, which lead to formation of mixed Ge-O-Te linkages and changes in the degree of modification of both network-forming oxides. Specifically, it was found that structural rearrangements in the tellurite part are related to the destruction of $TeO_{4/2}$ trigonal bipyramids and $(TeO_3)^{2-}$ trigonal pyramids in favor of TeO_{3+1} polyhedra. The corresponding changes in the germanate part involve the transformation of tetrahedral Q^3 units to octahedral GeO_6 units for M=Na and to tetrahedral Q^2 units for M=Li. These structural changes were expressed in terms of chemical equilibria which demonstrate the decrease

of modification in the tellurite part and its increase in the germanate part, in line with the basicity difference between the two glass-forming oxides.

The knowledge developed for the structures of the germanate and tellurite units in the studied binary and ternary germanotellurite glasses was employed to predict changes in the network cross-linking density upon mixing. It was found that the crosslinking density remains practically the same for M=Li and increases for M=Na. Such variations in network cross-linking were correlated with the composition dependence of the glass molar volume, which changes linearly for M=Li and shows a negative deviation from additivity for M=Na.

In addition, consideration of changes in the negative charge distribution and the network cross-linking density among the germanate and tellurite units allowed predictions, albeit of qualitative nature, for changes in the electrostatic, E_B, and the network-strain, E_S, parts of the activation energy for ion conduction. It was found that, for different structural reasons, the predicted changes in E_B and E_S appear to cancel out for both glass series. This is in line with the absence of a pronounced NFM effect in ionic conductivity in the studied glasses; the M=Li series shows a weak positive NFM effect whereas the M=Na series shows practically no NFM effect.

CRediT author contribution statement

N.S. Tagiara: Investigation, Writing - review & editing. **K.I. Chatzipanagis:** Investigation, Writing - review & editing. **H. Bradtmüller:** Investigation, Writing - review & editing. **A.C.M. Rodrigues:** Conceptualization, Investigation, Writing - review & editing, Funding acquisition. **Doris Möncke:** Conceptualization, Investigation, Writing - review & editing. **Efstratios I. Kamitsos:** Conceptualization, Supervision, Funding acquisition, Formal analysis, Writing - review & editing, Project administration.

Declaration of competing interest

The authors declare that they have no known competing financial interests or personal relationships that could have appeared to influence the work reported in this paper.

Acknowledgements

References

[1]   M. Schuch, C.R. Müler, P. Maass, and S.W. Martin, Mixed barrier model for the mixed glass former effect in ion conducting glasses, Phys. Rev. Lett. 102 (2008) 145902/1-4.

[2]   D. Zielniok, H. Eckert, and C. Cramer, Direct correlation between nonrandom ion hopping and network structure in ion-conducting borophosphate glasses, Phys. Rev. Lett. 100 (2008) 35901/1-4.

[3]   L.M. Funke, H. Bradtmüller, and H. Eckert, Recoupling dipolar interactions with multiple I=1 quadrupolar nuclei: A 11B{6Li} and 31P{6Li} rotational echo double resonance study of lithium borophosphate glasses, Solid State Nucl. Magn. Reson. 84 (2017) 143–150

[4]   J.C. Mauro, Statistics of modifier distributions in mixed network glasses, J. Chem. Phys. 138 (2013) 12A522/1-8.

[5]   C. Hermansen, X. Guo, R.E. Youngman, J.C. Mauro, M.M. Smedskjaer, and Y. Yue, Structure-topology-property correlations of sodium phosphosilicate glasses, J. Chem. Phys. 143 (2015) 064510/1-10.

[6]   W. Wang, R. Christensen, B. Curtis, S.W. Martin, and J. Kieffer, A new model linking elastic properties and ionic conductivity of mixed network former glasses, Phys. Chem. Chem. Phys. 20 (2018) 1629-1641.

[7]   P. Liu, K. Januchta, L.R. Jensen, M. Bauchy, and M.M Smedskjaer, Competitive effects of free volume, rigidity, and self-adaptivity on indentation response of silicoaluminoborate glasses. J. Am. Ceram. Soc. 103 (2020) 944–954.

[8]   B. Raguenet, G. Tricot, G. Silly, M. Ribes, A. Pradel, The mixed glass former effect in twin-roller quenched lithium borophosphate glasses, Solid State Ionics 208 (2012) 25–30.

[9]   D. Larink, H. Eckert, M. Reichert, S.W. Martin, Mixed network former effect in ion-conducting alkali borophosphate glasses: Structure/property correlations in the system $[M_2O]_{1/3}[(B_2O_3)_x(P_2O_5)_{1-x}]_{2/3}$ (M=Li, K, Cs), J. Phys. Chem. C. 116 (2012) 26162–26176.

[10]   Q.J. Zheng, R.E. Youngman, C.L. Hogue, J.C. Mauro, M. Potuzak, M.M. Smedskjaer, and Y.Z. Yue, Structure of boroaluminosilicate glasses: Impact of $[Al_2O_3]/[SiO_2]$ ratio on the structural role of sodium, Phys. Rev. B 86 (2012) 054203/1-12.

[11]   H. Eckert, Network former mixing (NFM) effects in ion-conducting glasses. Structure/property correlations studied by modern solid-State NMR techniques, Diffusion Foundations 6 (2015) 144-193.

[12]   H. Bradtmüller, A.C.M Rodrigues, H. Eckert, Network former mixing (NFM) effects in alkali germanotellurite glasses, J. Alloys Compd. 873 (2021) 159835.

[13]   E.I. Kamitsos, A.P. Patsis, and G.D. Chryssikos, Infrared reflectance investigation of alkali diborate glasses, J. Non-Cryst. Solids 152 (1993) 246-257.

[14]   A. Winterstein-Beckmann, D. Möncke, D. Palles, E.I. Kamitsos, and L. Wondraczek, Structure-property correlations in highly modified Sr, Mn-borate glasses, J. Non-Cryst. Solids 376 (2013)165-174.

[15]   E.I. Kamitsos, G.D. Chryssikos, A.P. Patsis, J.A. Duffy, Metal ion sites in oxide glasses. Relation to glass basicity and ion transport, J. Non-Cryst. Solids 196 (1996) 249-254.

[16]   E.I. Kamitsos, Y.D. Yiannopoulos, and J.A. Duffy, Optical basicity and refractivity of germanate glasses, J. Phys. Chem. B 106 (2002) 8988-8993.

[17]   N.S. Tagiara, E. Moayedi, A. Kyritsis, L. Wondraczek, and E.I. Kamitsos, Short-range structure, thermal and elastic properties of binary and ternary tellurite glasses, J. Phys. Chem. B 123 (2019) 7905-7918.

[18]   K.I. Chatzipanagis, N.S. Tagiara, D. Möncke, S. Kundu, A.C.M. Rodrigues, E.I. Kamitsos, Vibrational study of lithium borotellurite glasses, J. Non-Cryst. Solids 540 (2020) 120011.

[19]   N.S. Tagiara, D. Palles, E.D. Simandiras, V. Psycharis, A. Kyritsis, E.I. Kamitsos, Synthesis, thermal and structural properties of pure TeO_2 glass and zinc-tellurite glasses, J. Non-Cryst. Solids 457 (2017) 116–125.

[20]   E.I. Kamitsos, Infrared spectroscopy of glasses, in: M. Affatigato (Ed.), Modern Glass Characterization, John Wiley & Sons, New York, 2015, pp. 32-73 (Chapter 2).

[21]   N. Mochida, K. Takahashi, K. Nakata, S. Shibusawa, Properties and structure of binary tellurite glasses containing mono- and di-valent cations, J. Ceram. Soc. Jpn. 86 (1978) 316-326.

[22]   M.K. Murthy and J. Ip, Some physical properties of alkali germanate glasses, Nature 201 (1964) 285-286.

[23]   G.S. Henderson and H.M. Wang, Germanium coordination and the germanate anomaly, Eur. J. Mineral. 14 (2002) 733-744.

[24]   O.V. Mazurin, M.V. Streltsina, T.P. Shvaiko-Shvaikovskaya, Handbook of glass data. Part B, Single-component and binary non-silicate glasses, Elsevier, Amsterdam 1985.

[25]   M. de Oliveira, J.S. Oliveira, S. Kundu, N.M.P. Machado, A.C.M. Rodrigues, H. Eckert, Network former mixing effects in ion-conducting lithium borotellurite glasses: Structure/property correlations in the system $(Li_2O)_y[2(TeO_2)_x(B_2O_3)_{1-x}]_{1-y}$, J. Non-Cryst. Solids 482 (2018) 14–22.

[26]   E.I. Kamitsos, Y.D. Yiannopoulos, M.A. Karakassides, G.D. Chryssikos, and H. Jain, Raman and infrared structural investigation of $xRb_2O-(1-x)GeO_2$ glasses, J. Phys. Chem. 100 (1996) 11755-11765.

[27]   Y.D. Yiannopoulos, E.I. Kamitsos, and H. Jain, Structure of potassium germanate glasses by vibrational spectroscopy, in Physics and Applications of Non-Crystalline Semiconductors in Optoelectronics, A. Andriesh and M. Bertolotti (Eds.), NATO ASI Series/High Technology, Kluwer Academic Publ., Dordrecht, 1997, vol. 36, pp. 317-325.

[28]   T.N. Ivanova and V.N. Bykov, Raman spectroscopy of glasses and melts of the Na_2O-GeO_2 system, Russian Metallurgy (Metally) 2010 (2010) 678-680.

[29]   T. Furukawa, and W.B. White, Raman spectroscopic investigation of the structure and crystallization of binary alkali germanate glasses, J. Mater. Sci. 15 (1980) 1648-1662.

[30]   G.S. Henderson and M.E. Fleet, The structure of glasses along the Na_2O-GeO_2 join, J. Non-Cryst. Solids 134 (1991) 259-269.

[31]   G.S. Henderson, L.G. Soltay, and H.M. Wang, Q speciation in alkali germanate glasses, J. Non-Cryst. Solids 356 (2010) 2480-2485.

[32]   K. Nakamoto, Infrared and Raman Spectra of Inorganic and Coordination Compounds, Wiley, New York, 1978, p. 142.

[33] E.I. Kamitsos, Y.D. Yiannopoulos, C.P. Varsamis and H. Jain, Structure-property correlations in glasses by infrared reflectance spectroscopy, J. Non-Cryst. Solids 222 (1997) 59-68.

[34] E.I. Kamitsos, Y.D. Yiannopoulos, H. Jain and W.C. Huang, Far-infrared spectra of alkali germanate glasses and correlation with electrical conductivity, Phys. Rev. B 54 (1996) 9775-9783.

[35] L.L. Velli, C.P. Varsamis, E.I. Kamitsos, D. Möncke and D. Ehrt, Structural investigation of metaphosphate glasses, Phys. Chem. Glasses 46 (2005) 178-181.

[36] F. Dachille and R. Roy, The use of infra-red absorption and molar refractivities to check coordination, Z. Kristallogr. 111 (1959) 462-470.

[37] P. Tarte, Infra-red spectrum and tetrahedral coordination of lithium in the spinel $LiCrGeO_4$, Acta Crystallogr. 16 (1963) 228-228.

[38] P. Tarte and A.E. Ringwood, Infra-red spectrum and germanium co-ordination in some high-pressure meta-germanates, Nature 201 (1964) 819-819.

[39] T. Sekiya, N. Mochida, A. Ohtsuka, and M. Tonokawa, Raman spectra of $MO_{1/2}$-TeO_2 (M=Li, Na, K, Rb, Cs and Tl) glasses, J. Non-Cryst. Solids 144 (1992) 128-144.

[40] N. Ghribi, M. Dutreihl-Colas, J.-R. Duclére, T. Hayakawa, J. Carreaud, R. Karray, A. Kabadou, and P. Thomas, Thermal, optical and structural properties of glasses within the TeO_2-TiO_2-ZnO system, J. Alloys Comp. 622 (2015) 333-340.

[41] A. Kaur, A. Khanna, M. González-Berriuso, F. González, and B. Chen, Short-range structure and thermal properties of alumino-tellurite glasses, J. Non-Cryst. Solids 470 (2017) 14-18.

[42] P. Mosner, O. Kupetska, L. Koudelka, and P. Kalenda, Physical properties and structural studies of lithium borophosphate glasses containing TeO_2, J. Solid State Chem. 270 (2019) 547-552.

[43] A.G. Papadopoulos, N.S. Tagiara, E.D. Simandiras, E.I. Kamitsos, On the absence of doubly bonded Te=O groups in TeO_2 glass, J. Phys. Chem. B 124 (2020) 5746-5753.

[44] A. Pan and A. Ghosh, Activation energy and conductivity relaxation of sodium tellurite glasses, Phys. Rev. B 59 (1999) 899- 904.

[45] V. Dimitrov, S. Sakka, Electronic oxide polarizability and optical basicity of simple oxides, J. Appl. Phys. 79 (1996) 1736-1740.

[46] O.L. Anderson, D.A. Stuart, Calculation of activation energy of ionic conductivity in silica glasses by classical methods, J. Am. Ceram. Soc. 37 (1954) 573-580.

[47] H. Unuma, S. Sakka, Electrical conductivity in Na-Si-O-N oxynitride glasses, J. Mater. Sci. Lett. 6 (1987) 996-998.

[48] M. Dussauze, E.I. Kamitsos, P. Johansson, A. Matic, C.P. Varsamis, D. Cavagnat, P. Vinatier, and Y. Hamon, Lithium ion conducting boron-oxynitride amorphous thin films: Synthesis and molecular structure by infrared spectroscopy and density functional theory modelling, J. Phys. Chem. C 117 (2013) 7202-7213.

[49] W.C. Huang, H. Jain, Correlation between local structure and electrical response of Rb and (Rb,Ag) germanate glasses: dc conductivity, J. Non-Cryst. Solids 188 (1995) 254-265.

[50] H. Jain, W.C. Huang, E.I. Kamitsos, and Y.D. Yiannopoulos, Significance of intermediate range structure for electrical conduction in alkali germanate glasses, J. Non-Cryst. Solids 222 (1997) 361-368.

[51] M.M. Smedskajaer, J.C. Mauro, S. Se, J. Deubener, and Y. Yue, Impact of network topology on cationic diffusion and hardness of borate glass surfaces, J. Chem. Phys. 133 (2010) 154509/1-6.